# Viability of $ft$ Measurements with TAMUTRAP

Benjamin Schroeder

(Dated: May 27, 2020)

$\beta$ decays in TAMUTRAP have been simulated to determine the trap's potential to make $\beta$-delayed proton branching ratio measurements with improved precision. The simulations and analysis presented here demonstrate a relative uncertainty on the superallowed branch as low as $(0.19\%)_{\text{stat}} + (0.16\%)_{\text{sys}}$ if we are able to achieve 1 000 000 decays in the trap. This gives promise that TAMUTRAP will advance the precision frontier of $ft$ measurements for $^{32}$Ar, as well as other $T = 2,\ 0^+ \rightarrow T = 2,\ 0^+$ $\beta$-delayed proton emitters when they are available for study at the Cyclotron Institute.

## I. MOTIVATION AND BACKGROUND

$\beta$ decay has long served as a test of predictions made by the standard model and to search for physics beyond the standard model. The $T = 1,\ 0^+ \rightarrow 0^+$ superallowed $\beta$ emitters give the current best precision measurement of $V_{ud}$, the up-down element in the Cabibbo-Kobayashi-Maskawa (CKM) matrix.

The quantity measured for $V_{ud}$ experiments is the comparative half-life, $ft$, of the superallowed branch. This value is determined by two quantities: the statistical rate function, $f$, which is determined purely by the decay's end-point energy (or $Q$-value); and the partial half-life of the branch, $t$, which is determined by the half-life, $t_{1/2}$, and branching ratio to the daughter state of interest, $b$. To account for the small ($\sim 1\%$) differences in the isotopes arising from isospin and radiative corrections, the corrected $\mathcal{F}t$ value is instead used, which yields the relation to $V_{ud}$ [1]:

$$\mathcal{F}t = ft(1 + \delta'_R)(1 + \delta_{\text{NS}} - \delta_C) = \frac{K}{2G_V^2(1 + \Delta_R^V)}, \tag{1}$$

where $K = 8120.2776(9) \times 10^{-10}$ GeV$^{-4}$s, $\Delta_R^V$ is the transition-independent part of the radiative correction, $\delta'_R$ and $\delta_{\text{NS}}$ are the transition-dependent part of the radiative correction, and $\delta_C$ is the isospin-symmetry-breaking correction. The Conserved-Vector-Current hypothesis (CVC) demands that the coupling constant $G_V$ is indeed constant, and not renormalized in the nuclear medium. This has been verified to high precision with the $T = 1$ transitions, yielding the value of $V_{ud} = G_V/G_F$, where $G_F$ is the Fermi coupling constant of the electroweak interaction, and is well-determined from muon decay [2].

TAMUTRAP plans to study $\beta$ emitters far from stability, in the form of $T = 2,\ 0^+ \rightarrow 0^+$ $\beta$-

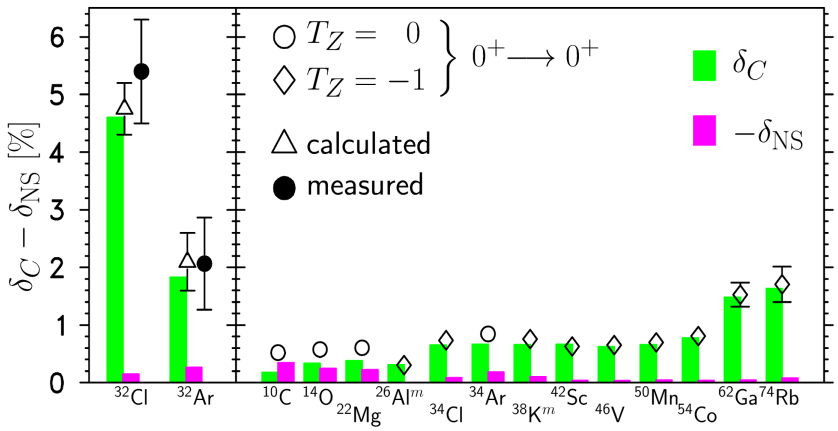


FIG. 1: The corrections $\delta_{\rm C}$, $\delta_{\rm NS}$ for the $T = 1$ isotopes used in the $V_{ud}$ survey (right [1]) and for $^{32}$Ar [3] and $^{32}$Cl [4] (left).

delayed proton emitters. The primary goal is to measure the $\beta$-$\nu$ angular correlation through the proton energy spectra, but this presents opportunity for a simultaneous measurement of branching ratios. These isotopes have large corrections in the $\mathcal{F}t$ values because they are far from stability (Fig. 1 illustrates the large corrections for $^{32}$Ar and $^{32}$Cl compared to the $T = 1$ isotopes used to test CVC and extract $V_{ud}$). This presents an opportunity to provide a benchmark for theoretical models: by comparing the $ft$ value for a particular transition to the $T = 1$ average, $\overline{\mathcal{F}t}$, one obtains an experimental measure of the correction,

$$\delta_C - \delta_{\rm NS} = 1 - \frac{\overline{\mathcal{F}t}}{ft(1+\delta'_R)}. \tag{2}$$

By measuring these corrections in cases where it is large, one may discern between competing models and ultimately reduce theoretical uncertainties in the $T = 1$ cases, improving the test of CVC and extraction of $V_{ud}$. TAMUTRAP plans to make this measurement for several isotopes, including $^{20}$Mg, $^{24}$Si, $^{28}$S, $^{32}$Ar, and $^{36}$Ca.

## II. EXPERIMENTAL DESCRIPTION

The TAMUTRAP Penning trap and beamline have been previously described [5, 6] It consists of a 37-segment radio-frequency quadrupole (RFQ) Paul trap which cools and bunches an ion beam, and the world's largest Penning trap [7], the geometry of which is shown in Fig. 2. The Penning trap is where ion masses are currently measured and where radioactive ion decay and measurements will occur once the TAMU Re-accelerated Exotic beam program (T-REX) is able to provide beams of $T = 2$, $0^+ \rightarrow T = 2$, $0^+$ $\beta$-delayed proton emitters at suitable intensities.

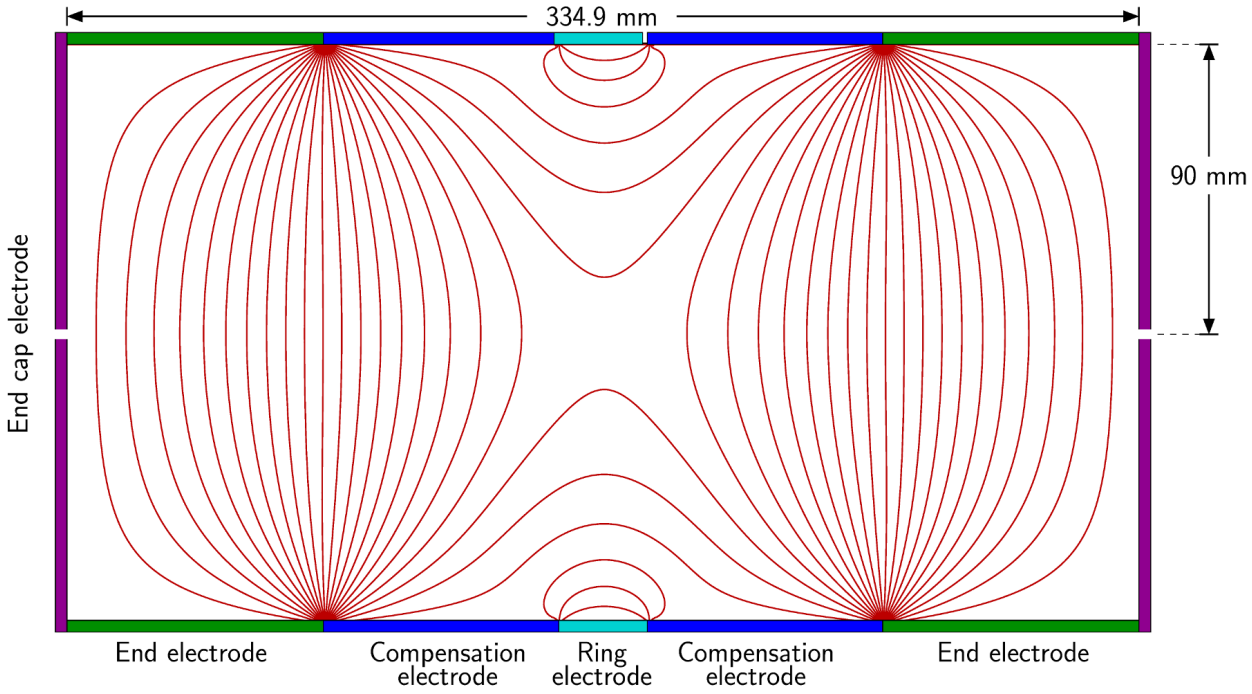


FIG. 2: The geometry of TAMUTRAP's electrodes. Contours of constant potential show the locally hypberbolic electric field. The magnetic field is along the central axis.

### A. Penning Trap Operating Principles and Mass Measurements

Penning traps combine a strong, homogeneous magnetic field with a relatively weak, hyperbolic electric field to trap charged particles in the trap center. The magnetic field on its own would tend to confine the trajectories of the charged particles to helices about the field axis, with angular frequency $\omega_c = \frac{qB}{m}$ and radius $r_c = \frac{v_\perp}{\omega_c}$ while the electric field on its own would act as a harmonic oscillator, with angular frequency $\omega_z = \sqrt{2qU_0/Md^2}$. Here $q$ is the charge of the ion, $B$ is the magnetic field, $m$ is the mass of the ion, $v_\perp$ is the radial velocity component (perpendicular to magnetic field), $U_0$ is the trapping potential, and $d = \sqrt{\frac{1}{2}(z_0^2 + \frac{1}{2}\rho_0^2)}$ is the characteristic dimension of the trap (with $z_0$ the inner half-length and $\rho_0$ the inner radius). When jointly applied, the equations of motion are coupled, leading to three eigenmotions:

- the transverse reduced cyclotron motion, with angular frequency $\omega_+ = \frac{\omega_c}{2}\left(1 + \sqrt{1 - 2(\frac{\omega_z}{\omega_c})^2}\right)$
- the transverse magnetron motion, with angular frequency $\omega_- = \frac{\omega_c}{2}\left(1 - \sqrt{1 - 2(\frac{\omega_z}{\omega_c})^2}\right)$, and
- the axial motion, with angular frequency $\omega_z$ as above.

The central "ring" electrode is segmented into four electrodes, and used as an antenna to excite the radial eigenmotions.

The contemporary standard application of Penning traps is the precision measurement of ion masses. Once ions are loaded in the trap, dipole and quadrupole signals are applied to the electrodes with the dipole near the magnetron frequency and the quadrupole near the cyclotron frequency. This combination allows energy to be transferred to the ions, converting magnetron motion to cyclotron motion. When the cyclotron resonance is reached, the ions gain maximal radial energy in the cyclotron mode, and are subsequently ejected by lowering the electric potential barrier. The (effective) magnetic moment of the ions is conserved, and as they travel from high magnetic field to low magnetic field their radial energy is converted into axial energy, which is seen as a drop in the time of flight of the ions from the trap to a detector far from the strong magnetic field region. This technique is especially robust, as an invariance theorem states that irrespective of misalignment between the trap axis and the magnetic field, the altered frequencies $\overline{\omega}_i$ satisfy the relation $\omega_c^2 = \overline{\omega}_+^2 + \overline{\omega}_-^2 + \overline{\omega}_z^2$ [8].

### B. $a_{\beta\nu}$ Measurements

The decays TAMUTRAP is designed to study are $\beta$-delayed proton emitters where the up to 4.3 MeV protons are fully contained by the 7 T field of the superconducting solenoid. The $T = 2$, $0^+ \rightarrow T = 2$, $0^+$ are of particular interest because their transition rates are theoretically well understood. The differential decay rate for unpolarized $\beta$-emitters (including the $T = 2,\ 0^+ \rightarrow T = 2,\ 0^+$ case here) is [9, 10],

$$\frac{d^5\Gamma}{dE_\beta d\Omega_\beta d\Omega_\nu} \propto F(\pm Z, E_\beta) p_\beta E_\beta (A_0 - E_\beta)^2 \left[1 + a_{\beta\nu}\frac{\vec{p}_\beta \cdot \vec{p}_\nu}{E_\beta E_\nu} + b_F \frac{m_e}{E_\beta}\right]. \tag{3}$$

Here $p_i, E_i$ are the momenta and total energy of the $i = \beta, \nu$, $F(Z, E_\beta)$ is the Fermi function, $A_0$ is the kinematically-determined energy cutoff for the $\beta$, $a_{\beta\nu}$ is the $\beta$-$\nu$ angular correlation parameter, and $b_F$ is the Fierz parameter. In terms of the fundamental vector and scalar coupling constants ($C_V$ and $C_S$ respectively), the correlation parameters for $0^+ \rightarrow 0^+$ transitions are given by [9, 10]:

$$a_{\beta\nu} = \frac{|C_V|^2 + |C_V'|^2 - |C_S|^2 - |C_S'|^2}{|C_V|^2 + |C_V'|^2 + |C_S|^2 + |C_S'|^2} \tag{4}$$

and

$$b_F = \frac{-2\Re e(C_S^* C_V + C_S'^* C_V')}{|C_V|^2 + |C_V'|^2 + |C_S|^2 + |C_S'|^2} \tag{5}$$

In the Standard Model, $C_S = C_S' = 0$ reflecting the absence of scalar currents, leading to $a_{\beta\nu} = 1$ and $b = 0$. Thus a measurement of $a_{\beta\nu} < 1$ and $b_F \neq 0$ would be a clear indication of a scalar interaction beyond the standard model's $V - A$ form for the weak interaction.

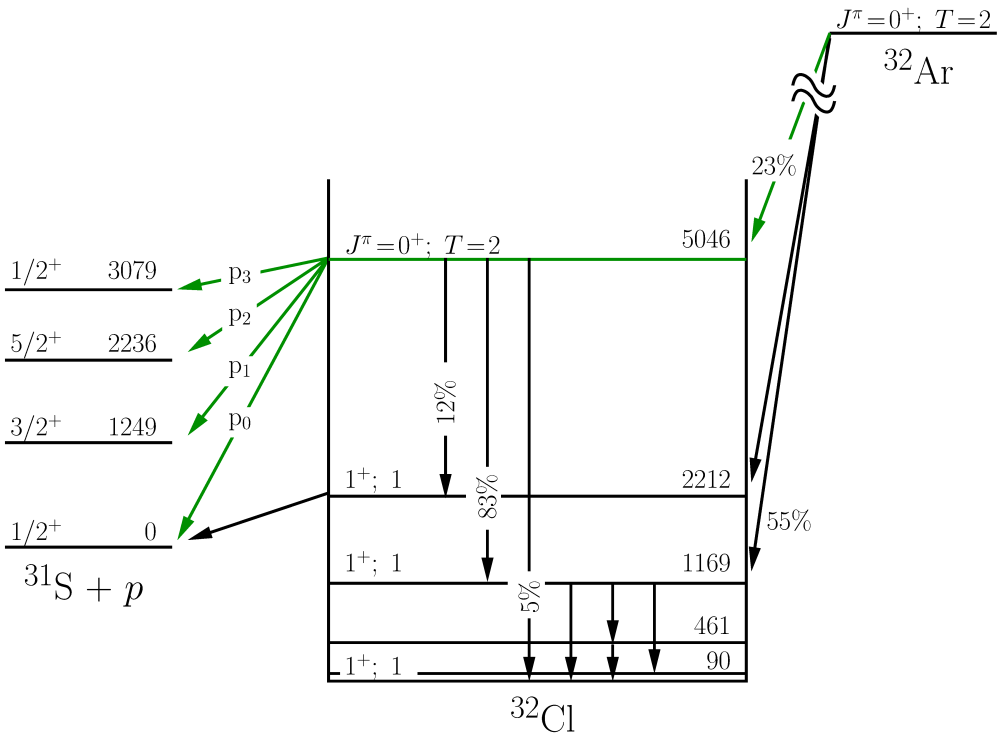


FIG. 3: A simplified decay scheme for the decay of $^{32}$Ar [3]. The superallowed branch ($E_{\rm exc} = 5.046$ MeV, highlighted in green) has four possible proton emissions, as well as $\gamma$ branches to other $^{32}$Cl states.

One of the physics goals of the TAMUTRAP facility is to measure the $a_{\beta\nu}$ parameter. Due to the low interaction cross sections of neutrinos, they will be infeasible to detect directly. In principle, one could measure the recoiling ion as a surrogate, however the kinetic energies of the recoiling nuclei are small, $\lesssim 2$ keV for the isotopes of interest. This energy is difficult to detect with silicon detectors, so this is not the measurement which will be made.

Instead, TAMUTRAP relies on the Doppler shift of the energy of particle emission. The isotopes of interest are $\beta$-delayed proton emitters (see Fig. 3), where the intermediate nucleus after $\beta$ decay is short-lived ($t_{1/2} < 10^{-12}$ s) and decays into a daughter nucleus and a proton with a line energy in the center-of-mass frame. Since the intermediate is so short-lived, the recoil momentum is unchanged between the $\beta$-decay and proton emission. Then once the proton is emitted, it will have a small energy shift as seen in the lab due to the moving center-of-mass inertial frame.

In the case of the standard model ($a_{\beta\nu} = 1$), the decay rate is maximized at $\theta_{\beta\nu} = 0$, corresponding to the largest recoil momentum. The resulting energy spectrum is a broad peak. In the maximally standard-model-violating case ($a_{\beta\nu} = -1$), the decay rate is maximized at $\theta_{\beta\nu} = \pi$, corresponding to zero recoil momentum, and the resulting spectrum is a sharper peak. Figure 4

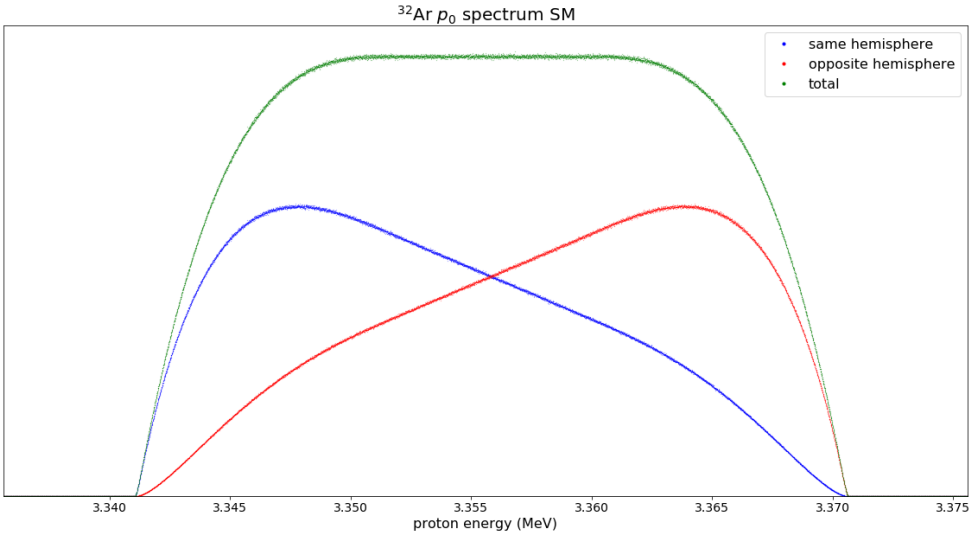


FIG. 4: The spectra of the $p_0$ proton energies when the protons are detected in the same hemisphere and opposite hemisphere as the coincident $\beta$s.

shows the spectra for the standard model case.

To measure this, the end-cap electrodes in TAMUTRAP will ultimately be replaced with double-sided silicon-strip detectors (DSSDs). The radioactive ions in charge state +1 will be loaded into the trap then moved away from the axis with the radio-frequency excitation. Once the ions decay, the $\beta$ particles will travel in a helix with Larmor diameter $d \leq 11$ mm, resulting in an annular band of hits on the detector; the protons will travel in a much wider helix due to their low energy and high mass, with Larmor diameter $d_p \lesssim 85.4$ mm (for the dominant 4.28 MeV peak in $^{20}$Mg; it is smaller for the other, lower energy proton peaks), resulting in a broad distribution several radial peaks as seen in Fig. 5.

In order to inject ions, the DSSDs will have central holes with diameters of approximately 5 mm; the exact dimension will be determined as the detector geometry is finalized. Due to the central holes and the 11 mm limit on the radial distance from the decay position to the $\beta$ position, a large fraction of the $\beta$ particles would be lost through the central hole if the $^{32}$Ar ions were to decay from the trap center. To avoid this, the ions will be moved off the central axis by exciting the $\omega_{\pm}$ eigenmotions. The position distribution of the ions has not yet been determined (and cannot be until the beam characteristics provided by T-REX are known), but the mass measurements thus far have demonstrated the ability to efficiently excite the eigenmotions.

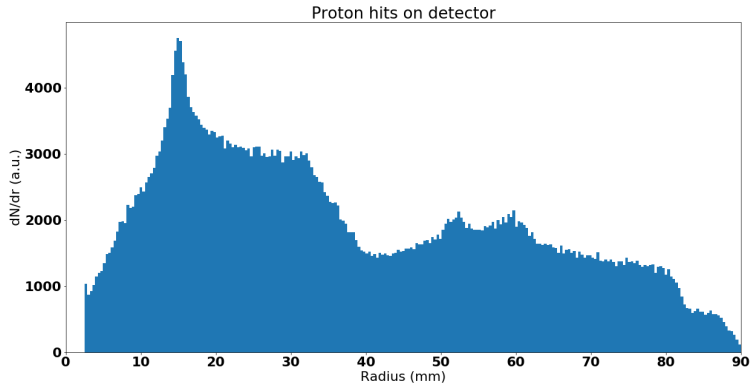


FIG. 5: The radial distribution of protons on the detectors. For this simulation, the original ion position is on a cylindrical shell of inner radius 13.5 mm and outer radius 16.5 mm.

### C. $ft$ Measurements

Measuring these protons provides another opportunity–measuring the comparative half-lives, $ft$, of the $\beta$ transitions. The comparative half-life is defined as the product

$$ft = f(Q_{\mathrm{EC}}; Z)\frac{t_{1/2}}{b}, \tag{6}$$

where $t_{1/2}$ is the total half-life of the isotope, $b_i$ is the branching ratio of the decay channel, $f$, the statistical rate function, is the integral of the phase-space factor of Eq. (3), and depends only on the atomic number and the cutoff energy of the decay channel, $Q_{\mathrm{EC}}$ [1].

The current uncertainty budget for the superallowed $ft$ of $^{32}$Ar is 0.017% due to $Q_{\mathrm{EC}}$, 0.3% due to the half-life, and 0.7% due to the branching ratio [3]. The TAMUTRAP target for $ft$ is to reduce the branching ratio to the 0.1% level.

The superallowed branching ratio is given by

$$\begin{aligned} b_{\mathrm{SA}} &= \frac{N_{\mathrm{SA}}}{N_{\mathrm{tot}}} \\ &= b_{\mathrm{SA}}^{\beta p} + b_{\mathrm{SA}}^{\beta\gamma} = \frac{N_{\mathrm{SA}}^{\beta p}}{N_{\mathrm{tot}}} + \frac{N_{\mathrm{SA}}^{\beta\gamma}}{N_{\mathrm{tot}}}, \end{aligned} \tag{7}$$

where $b_{\mathrm{SA}}^{\beta p}$ is the branching ratio for all superallowed $\beta$-delayed proton emission branches and $b_{\mathrm{SA}}^{\beta\gamma}$ is the superallowed branching ratio for all $\beta\gamma$ decays, where the daughter nucleus decays to the ground state rather than proton emission, $N_{\mathrm{SA}}$ is the number of decays through the superallowed channel, and $N_{\mathrm{tot}}$ is the total number of decays.

In TAMUTRAP, the same silicon detectors will capture both the full energy of the proton and the deposited energy of the $\beta$s. The narrow (30 keV full width) superallowed proton peaks will

be measured with high energy resolution for the $a_{\beta\nu}$, and will be easily distinguished from the continuum of $\Delta E$s of the $\beta$s, yielding $N_{\mathrm{SA}}^{\beta p}$.

TAMUTRAP is designed as a charged particle detector, and will not be able to make measurements of $\beta\gamma$ branches, so TAMUTRAP will only be able to improve the precision of $b_{\mathrm{SA}}^{\beta p}$. The remainder of the measurement is the normalization factor, $N_{\mathrm{tot}}$. The energy of the injected ions is limited by the trap depth, which has been kept near 200 V for stable ions in TAMUTRAP; this makes it difficult to count the number of incoming ions as they enter the trap, so the normalization must come from the $\beta$ count.

One complication of this is the radioactivity of the intermediate nuclei. Though the isobaric analog state (IAS) branches leave the daughter nucleus above the proton separation energy, there are still significant $\beta\gamma$ branches, in addition to the possibility that the $^{32}$Ar decays to some state other than the IAS, leaving the radioactive daughter nucleus below the separation energy. These nuclei will undergo a second $\beta$ decay, and contaminate the $\beta$ spectrum of the parent isotope. Though these daughter isotopes are more stable than their parents, the half-lives vary from 2 to 4.8 times longer than the parent (except for $^{24}$Si, with a ratio of 14.7), so contamination is expected.

This concern is partially mitigated by the trapping scheme. The ions injected to the Penning trap are prepared in the +1 charge state, so after the $\beta^+$ decay many daughter nuclei will be in neutral atoms. Those recoils which are in neutral atoms will not be affected by the trapping fields, and will travel in uniform distribution over $4\pi$ before implanting on an electrode or detector and ultimately decaying at rest. This will create a spectrum on the detectors with density $\sim r$, in contrast to the sharp ring of the $\beta$s from the parent decays as seen in Fig. 6. In the case that there are shakeoff electrons and the daughter ion is in a positive charge state, the ion may be trapped, however the electric potential depth is adjustable so making the well shallower may further reduce any daughter decay contamination. There is an additional peak from the contaminants at the full radius of the detector due to those ions which implant on a trap electrode at the same radius.

## III. SIMULATIONS

The simulation work for this project has two main components: (1) a Monte Carlo $\beta$ decay event generator, which generates $\beta$ decays randomly with importance sampling, and (2) a Geant4 simulation, which implements the experimental geometry, tracks the decay products' trajectories, and simulates their interaction with matter.

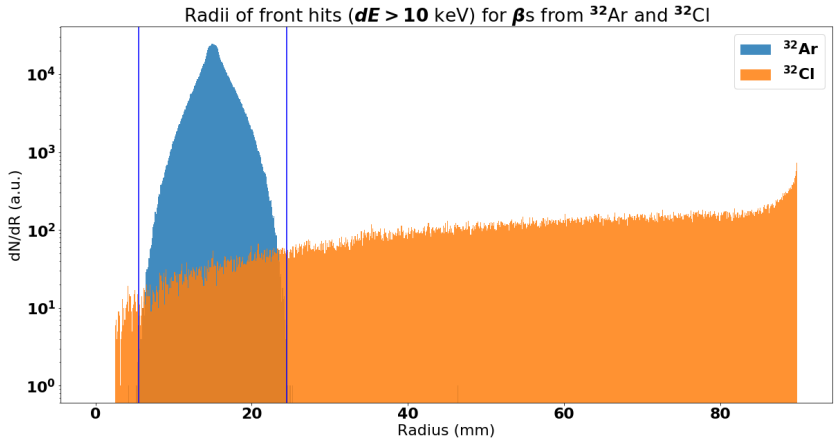


FIG. 6: The positional spectra of $\beta$ hits from $^{32}$Ar and $^{32}$Cl on the detectors. Note the logarithmic scale of the y-axis. The vertical lines denote the $^{32}$Ar counting region.

### A. Monte Carlo Event Generator

The Monte Carlo generator is a C++ library which generates representative samples of $\beta$-delayed proton emission events. Since the phase space is large, the generator cannot sample the entire phase space, so importance sampling is used to make the sample representative of the differential decay rate distribution. Once the decay parameters are set, the generator creates $\beta$-decay events by selecting energetically-allowed momenta for the $\beta$ and $\nu$ and calculating the differential decay rate Eq. (3) for those momenta. The samples are then accepted or rejected based on an initialization sample of the phase space, where 100 000 events are generated and the maximum decay rate $d\Gamma_{max}$ of the sample is stored and multiplied by a factor $\alpha = 1.1$ to account for the overwhelmingly likely case that the sample does not include the exact maximum decay rate.

After the initialization, events are generated in the same manner, then accepted or rejected with probability $p = \frac{1}{\alpha}\frac{d\Gamma}{d\Gamma_{\max}}$. This ensures the samples generated are representative of the true distribution of momenta based on the differential decay rate, and these samples are usable for calculating observable quantities. The $\beta$ energy spectrum of the $^{32}$Ar superallowed branch computed with this library is shown in Fig. 7.

The generator also includes proton emission: after generating a $\beta$ event, a proton of a chosen branch is emitted in a random direction with the energy given by single-body decay, then boosted back into the lab frame and recorded. The energy spectra for the $p_0$ branch, $^{32}\text{Ar} \rightarrow {}^{32}\text{Cl}$ (5.046 MeV) $\rightarrow {}^{31}\text{S(g.s.)} + p$, are shown in Fig. 4.

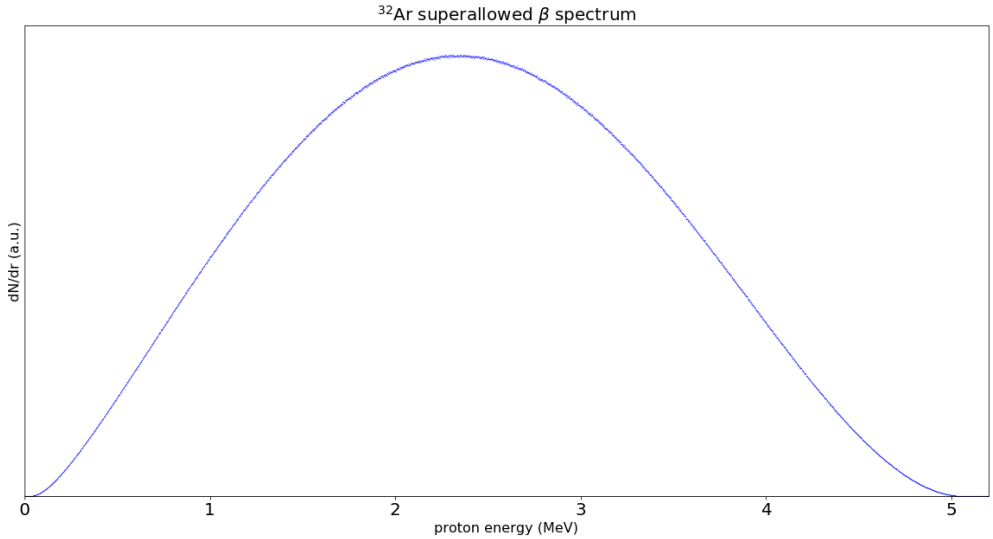


FIG. 7: The simulated energy spectrum of the $^{32}$Ar 5.046 MeV superallowed branch.

### B. Geant4

The TAMUTRAP experiment is simulated in Geant4 [11–13] to account for particle transport and interaction with matter. The simulation defines a simplified version of the geometry used in TAMUTRAP with the end-cap electrodes replaced by silicon `G4SensitiveDetector`.

The simulation is divided into events, with each event corresponding to the decay of a single $^{32}$Ar ion through a selected branch. The decay radiation particles (either a $\beta$ and a proton or a $\beta$ and a radioactive $^{32}$Cl atom) are generated by the $\beta$ event generator and input to Geant. Though the initial position distribution of the ions has not yet been determined, a cylindrical shell has been chosen with axial length of the ring electrode, inner radius 13.5 mm, and outer radius 16.5 mm. These parameters are chosen such that none of the $^{32}$Ar $\beta$s escapes the central hole, and with the assumption that the radial spread after excitation is similar to the bunch size, which is limited by the currently-coded 5 mm central holes of the detectors.

Once the particles have been initialized, Geant tracks them until their kinetic energy drops below a threshold (chosen to be 100 eV) or they exit the simulation volume (a 10 m cube centered about the trap center). For each simulation step that the particles travel through the detector, the position and deposited energy is recorded. Ultimately, for each event each detector records the energy deposited by each primary particle (plus the energy deposited by the secondary electrons it creates) and the average position of these hits for post-simulation analysis.

## IV. ANALYSIS

For this $ft$ analysis, the Geant simulation was run to generate 1 000 000 events in the superallowed $\beta\gamma$ branch.

### A. Backscattering

Because $\beta$s are much lighter than the atoms in scattering surfaces, they have high backscatter rate compared with ions. In TAMUTRAP this is exasperated by the $4\pi$ nature of the system: particles incoming to the detector have a $\cos\theta$ distribution, so a large fraction of particles have are far from normal incidence, and do not require as large a scattering angle to be backscattered.

Due to the unusually high backscatter rate, the simulation was benchmarked against experimental data and other simulations used as validation tests of Geant4 [14]. A new geometry was made for the simulation, comprising a pencil beam of electrons incident on a surface. This was repeated for thin and semi-infinite geometries, varying over several materials and angles of incidence. As Geant4 is developed by CERN, the default settings are optimized for high-energy experiments so the `G4PhysicsList` was additionally varied between the default `G4EmStandardPhysics`, `G4EmStandardPhysics_opt3`, and `G4EmStandardPhysics_opt4`; the latter two are more accurate than the default, with computation time as a trade-off. After comparing the results, `G4EmStandardPhysics_opt4` was selected and used for the simulation, as it provided closest agreement with the external data.

After including these changes, the backscatter rate was found to be 17.4% for the $\beta$ spectrum for the superallowed branch. Despite the high backscatter rate double counting can be mitigated with counting techniques, as will be discussed in IV B.

### B. Coincidence

The lifetime of the IAS is quite short, $\lesssim 10^{-12}$ s, so the creation of the $\beta$ and proton at the same time in the $\beta p$ branch simulation is reasonable. The inner length of the trap (detector-to-detector) is 33.489 mm $\approx$ 1.1 ns $\cdot c$, setting the minimum time-of-flight for the $\beta$s. The protons are nearly mono-energetic; in the case of $^{32}$Ar, their speed is $0.084c$, making their minimum time-of-flight $\approx$ 12 ns.

Due to their helical motion in the magnetic field, each proton and $\beta$ has its time-of-flight delayed by a factor of $\sec\theta$, where $\theta$ is the pitch angle (0 for a straight line). Comparing with the actual $\beta$

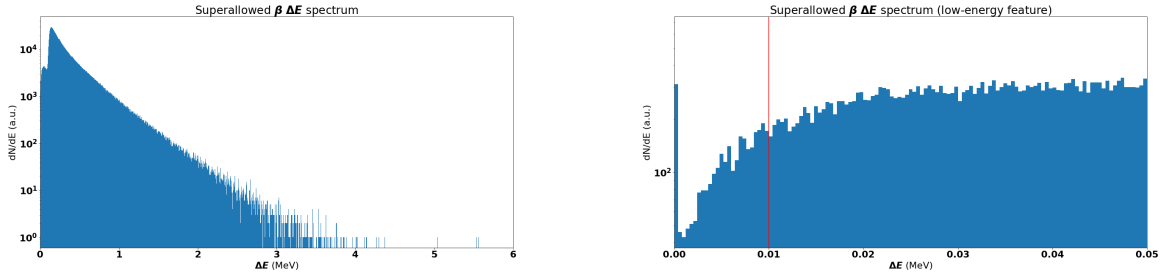


(a) Full $\Delta E$ spectrum for $^{32}$Ar superallowed branch ($Q_{\mathrm{EC}} = 6.088$ MeV).

(b) Low energy $\Delta E$ spectrum with 10 keV cutoff used in analysis.

FIG. 8: $\Delta E$ spectrum of the $\beta$ hits from $^{32}$Ar superallowed branch in the DSSD.

times-of-flight, we see a distribution agreeing with these observations. Looking at the actual time-of-flight difference from the coincident event, we find that all of the detected events would have coincident time-difference between 1.1 and 100 ns. We anticipate fewer than 1000 ions per bunch loaded into the trap, so the average time between successive decays is $\sim \tau/N = 98$ $\mu$s for $^{32}$Ar. Because this is three orders of magnitude greater than the $\beta$ timing and the protons have very narrow energy peaks, we conclude that the proton signals will be identified with the corresponding $\beta$ signals from the same decay.

### C. Energy thresholds

In the case of protons there is no need for energy thresholds, as the silicon detector thickness is chosen to be thick enough to completely stop them. Since $\beta$s are light their deposited energy spectrum ranges from 0 to the full energy; however, silicon strip detectors have dead layers near the surface which prevent full charge collection, so a minimum energy-deposit must be chosen.

Figs. 8a and 8b show the spectra of deposited energies $^{32}$Ar $\beta$s through the superallowed branch. A threshold of 10 keV was selected for this analysis, which captures all but 0.23% of $\beta$ hits (2968/1299757). All further analysis was made with this threshold.

### D. Position cuts

The radial distributions of the $\beta$ hits from $^{32}$Ar and $^{32}$Cl, shown in Fig. 6, have distinct shapes as discussed in II C. This allows for position cuts to be made to partially separate the two distribu-

tions. In this analysis cuts were made to capture the entire radial distribution of the superallowed $\beta$ hits (5.5 mm and 24.5 mm), except for a small number of outliers.

These cuts result in a contamination of $6357/982\,007 = 0.647\%$ $^{32}$Cl hits in the $^{32}$Ar region.

## V. RESULTS

The $\beta$-$p$ superallowed branching ratio is given by

$$b \triangleq b_{\mathrm{SA}}^{\beta p} = \frac{N_{\mathrm{SA}}^{\beta p}}{N_{\mathrm{SA}}^{\beta p} + N_{\mathrm{nonSA}}^{\beta p} + N^{\beta\gamma}}, \tag{8}$$

where $N_{\mathrm{SA}}^{\beta p}$ is the number of $\beta p$ transition through the superallowed state, $N_{\mathrm{nonSA}}^{\beta p}$ is the number of $\beta p$ transitions not involving the superallowed transition, and $N^{\beta\gamma}$ is the total number of $\beta\gamma$ transitions, where no proton is emitted. $N = N_{\mathrm{SA}}^{\beta p} + N_{\mathrm{nonSA}}^{\beta p} + N^{\beta\gamma}$ is the total number of ions that decay in the trap, and $b_i = N_i/N$ are the branching ratios. The uncertainty is given by

$$\begin{aligned}(\delta b)^2 &= \left(\frac{\partial b}{\partial N_{\mathrm{SA}}^{\beta p}}\delta N_{\mathrm{SA}}^{\beta p}\right)^2 + \left(\frac{\partial b}{\partial N_{\mathrm{nonSA}}^{\beta p}}\delta N_{\mathrm{nonSA}}^{\beta p}\right)^2 + \left(\frac{\partial b}{\partial N^{\beta\gamma}}\delta N^{\beta\gamma}\right)^2 \\ &= \left(\frac{N_{\mathrm{nonSA}}^{\beta p} + N^{\beta\gamma}}{N^2}\sqrt{N_{\mathrm{SA}}^{\beta p}}\right)^2 + \left(\frac{N_{\mathrm{SA}}^{\beta p}}{N^2}\sqrt{N_{\mathrm{nonSA}}^{\beta p}}\right)^2 + \left(\frac{N_{\mathrm{SA}}^{\beta p}}{N^2}\delta N^{\beta\gamma}\right)^2 \end{aligned} \tag{9}$$

Here it is assumed that the uncertainties $\delta N_i^{\beta p}$ associated with the proton branches are given by the square root of the number of counts as expected based on Gaussian statistical uncertainties as we expect unambiguous detection based on the narrow proton peaks. Simplifying Eq. (9) yields

$$\begin{aligned}(\delta b)^2 &= \left(\frac{1-b}{N}\right)^2 N_{\mathrm{SA}}^{\beta p} + \left(\frac{b}{N}\right)^2 N_{\mathrm{nonSA}}^{\beta p} + \left(\frac{b}{N}\right)^2 \left(\delta N^{\beta\gamma}\right)^2 \\ \left(\frac{\delta b}{b}\right)^2 &= \frac{(1-b)^2}{bN} + \frac{b_{\mathrm{nonSA}}^{\beta p}}{N} + (b^{\beta\gamma})^2 \left(\frac{\delta N^{\beta\gamma}}{N^{\beta\gamma}}\right)^2 \end{aligned} \tag{10}$$

Note that $\delta N^{\beta\gamma}$ requires more careful consideration than the proton branches because of the more involved counting scheme involving detector thresholds and conditions imposed when filtering the data. We will write

$$N^{\beta\gamma} = \frac{n_{\mathrm{det}}^{\beta\gamma}}{\varepsilon_{\mathrm{geo}}\varepsilon_{\mathrm{en}}} f_{\mathrm{pure}} \tag{11}$$

Here $\varepsilon_{\mathrm{geo}}$ is the fraction of $^{32}$Ar $\beta$s which fall in the counting region, $\varepsilon_{\mathrm{en}}$ is the fraction of $\beta$s above the energy threshold, $f_{\mathrm{pure}} = N_{\mathrm{Ar}}/(N_{\mathrm{Ar}} + N_{\mathrm{Cl}})$ is the purity fraction of $^{32}$Ar $\beta$s relative to $^{32}$Cl $\beta$s in the region, and $n_{\mathrm{det}}^{\beta\gamma}$ is the number of $\beta$ events detected satisfying the gate conditions:

1. No coincident proton

TABLE I: Systematic uncertainties associated with $N^{\beta\gamma}$ as defined in Eq. (11). All values are in percent.

| Quantity | Value | Uncertainty |
|---|---|---|
| $f_{\text{pure}}$ | 99.35 | 0.032 |
| $\varepsilon_{\text{geo}}$ | 97.57 | 0.004 |
| $\varepsilon_{\text{en}}$ | 99.77 | 0.16 |

2. Above the energy threshold
3. In the $^{32}$Ar $\beta$ counting region

From here we can calculate

$$\left(\delta N^{\beta\gamma}\right)^2 = \left(\frac{f_{\text{pure}}}{\varepsilon_{\text{geo}}\varepsilon_{\text{en}}}\delta n_{\text{det}}^{\beta\gamma}\right)^2 + \left(\frac{n_{\text{det}}^{\beta\gamma}}{\varepsilon_{\text{geo}}\varepsilon_{\text{en}}}\delta f_{\text{pure}}\right)^2 + \left(\frac{n_{\text{det}}^{\beta\gamma} f_{\text{pure}}}{\varepsilon_{\text{geo}}^2\varepsilon_{\text{en}}}\delta\varepsilon_{\text{geo}}^2\right)^2 + \left(\frac{n_{\text{det}}^{\beta\gamma} f_{\text{pure}}}{\varepsilon_{\text{geo}}\varepsilon_{\text{en}}^2}\delta\varepsilon_{\text{en}}\right)^2 \tag{12}$$

or

$$\left(\frac{\delta N^{\beta\gamma}}{N^{\beta\gamma}}\right)^2 = \left(\frac{\delta n_{\text{det}}^{\beta\gamma}}{n_{\text{det}}^{\beta\gamma}}\right)^2 + \left(\frac{\delta f_{\text{pure}}}{f_{\text{pure}}}\right)^2 + \left(\frac{\delta\varepsilon_{\text{geo}}}{\varepsilon_{\text{geo}}}\right)^2 + \left(\frac{\delta\varepsilon_{\text{en}}}{\varepsilon_{\text{en}}}\right)^2 \tag{13}$$

In order to calculate the systemic uncertainties of the simulation results, the cuts applied to the $^{32}$Ar counting region were varied. For the geometric factor, the upper and lower bounds of the radial cutoff were simultaneously varied by $\pm 0.5$ mm, i.e. $r_{\text{min}} = 5.5 \pm 0.5$ mm and $r_{\text{max}} = 24.5 \mp 0.5$ mm, and the half-width of the variation is reported as uncertainty; the purity fraction uncertainty was taken as its half-width within the same geometric cuts; and the energy threshold factor was taken as its half-width after varying by $\pm 5$ keV. Since $n_{\text{det}}^{\beta\gamma}$ is the quantity to be measured in experiment, its uncertainty is taken as the Gaussian error $\sqrt{n_{\text{det}}^{\beta\gamma}}$. This is $\lesssim \sqrt{N^{\beta\gamma}} = \sqrt{b^{\beta\gamma}N}$, so we use this more convenient quantity as a conservative estimate. The final values taken for these factors are given in Table I.

Returning with these to the total uncertainty and plugging in the literature values, $b = 20.83\%$, $b_{\text{nonSA}}^{\beta p} = 14.75\%$, and $b^{\beta\gamma} = 64.42\%$, we find:

$$\begin{aligned}\left(\frac{\delta b}{b}\right)^2 &= \frac{0.6268}{0.2083 \times N} + \frac{0.1475}{N} + \frac{0.6442}{N} + \left(\frac{0.032}{99.35}\right)^2 + \left(\frac{0.004}{97.57}\right)^2 + \left(\frac{0.16}{99.77}\right)^2 \\ &= \frac{3.80}{N} + (0.00164)^2\end{aligned} \tag{14}$$

Thus, the systematic uncertainty is $(\delta b)_{\rm sys} = 0.033\%$. If we are able to reach statistics of $N = 1\,000\,000$ total $^{32}$Ar decays in the trap, the total uncertainty will be $\delta b = 0.05\%$. This is well below the current value, and would lead to a very interesting comparison of calculations of isospin symmetry breaking. In conjunction with similar uncertainties expected from the other nuclei of the TAMUTRAP program ($^{20}$Mg, $^{24}$Si, $^{28}$S, $^{36}$Ca), the results could help discern between competing models and reduce theoretical uncertainties in the $T = 1$ cases.

## VI. ONGOING WORK

TAMUTRAP has been commissioned in an offline mode where radioactive isotopes are not available, but stable sources of the alkali metal ions $^{23}$Na, $^{37}$K, $^{85,87}$Rb, and $^{133}$Cs have been used to perform mass measurements with a precision of 30 parts per billion. In doing so a novel, single-trap purification technique has been developed to separate the two rubidium isotopes for mass measurement.

The silicon detectors have not yet been designed beyond a minimum thickness. To that end additional simulations and analysis are required to determine the ideal geometry of the detector bulk and strips. The major design considerations are:

- The radial pitch will directly affect radial resolution, and thus the ability to geometrically separate the $^{32}$Ar $\beta$s from those of $^{32}$Cl.

- The number of "pie slice" sections may be important in avoiding signal pileup with the high backscatter rate.

- The inner diameter of the active area determines the geometric efficiency of proton collection, and must be minimized (subject to a beamline alignment/optics requirement of $d_{\rm min} \gtrsim 2$ mm). It is not immediately clear how far a defect will affect the detector characteristics, so the difference between the central hole and the active area is a question of manufacturing.

- The $a_{\beta\nu}$ measurement requires measuring two proton spectra which are 1% features, with a full width of 30 keV on a 3.35 MeV signal. The Fano limit of energy resolution for silicon detectors at room temperature is on the order of 1 keV for 3.35 MeV peaks, so cooling the detectors should be considered if the energy resolution is the limiting factor. This will be a great design demand with the limited space inside the magnet bore.

- The simulation has included a second pair of detectors, outside the trap from the main detectors. This is an effort to better characterize backscatters: in the $ft$ measurement it is sufficient to identify a backscatter to avoid double-counting, but in the $a_{\beta\nu}$ measurement the events must be binned based on which hemisphere the $\beta$ hits first. If timing resolution is insufficient with one pair of detectors, then including this second pair may improve identification efforts. If one pair is sufficient, the second pair should be excluded to minimize backscattering.

[1] J. C. Hardy and I. S. Towner, Phys. Rev. C **91**, 025501 (2015).

[2] M. Tanabashi *et al.* (Particle Data Group), Review of particle physics, Phys. Rev. D **98**, 030001 (2018).

[3] M. Bhattacharya *et al.*, Physical Review C **77**, 065503 (2008).

[4] D. Melconian *et al.*, Phys. Rev. C **85**, 025501 (2012).

[5] M. Mehlman, *Development of the TAMUTRAP Facility for Precision Beta-Decay Studies*, Ph.D. thesis, Texas A&M University (2015).

[6] M. Mehlman *et al.*, Nuclear Instruments and Methods in Physics Research Section A **712**, 9 (2013).

[7] P. D. Shidling *et al.*, in *7th International Conference on Trapped Charged Particles and Fundamental Physics (TCP2018)*, Vol. 240 (2019) p. 40.

[8] L. S. Brown and G. Gabrielse, Geonium theory: Physics of a single electron or ion in a penning trap, Rev. Mod. Phys. **58**, 233 (1986).

[9] J. Jackson, S. Trieman, and H. Wyld, Nucl. Phys. A **4**, 206 (1957).

[10] J. Jackson, S. Trieman, and H. Wyld, Phys. Rev. **106**, 517 (1957).

[11] S. Agostinelli *et al.*, Nuclear Instruments and Methods in Physics Research Section A **506**, 250 (2003).

[12] J. Allison *et al.*, IEEE Transactions on Nuclear Science **53**, 270 (2006).

[13] J. Allison *et al.*, Nuclear Instruments and Methods in Physics Research Section A **835**, 186 (2016).

[14] P. Dondero *et al.*, Nuclear Instruments and Methods in Physics Research Section B **425**, 18 (2018).